IPCC-rapport Sea Level Rise / Hints:

- ⇨ Manueel aan te duiden op jullie print.

1 horizontaal

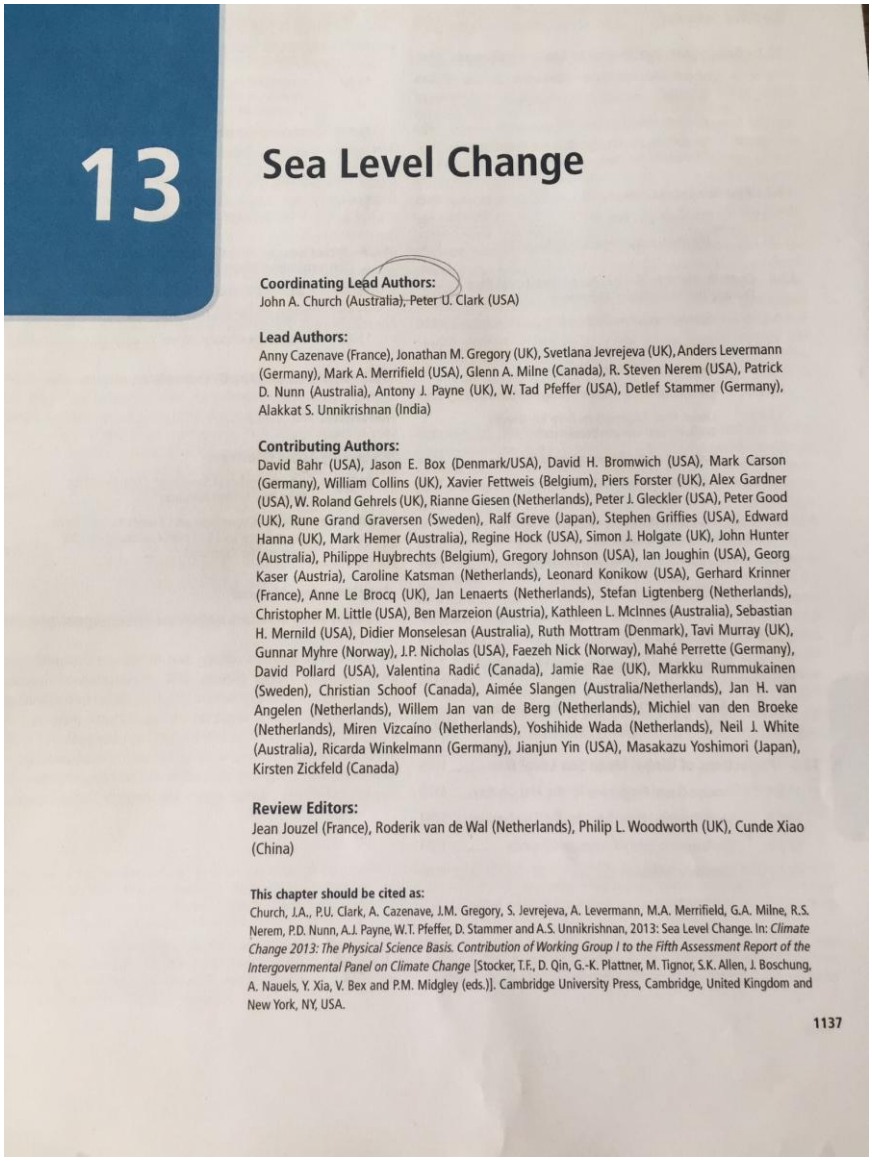

13 Sea Level Change

Coordinating Lead Authors:
John A. Church (Australia), Peter U. Clark (USA)

Lead Authors:
Anny Cazenave (France), Jonathan M. Gregory (UK), Svetlana Jevrejeva (UK), Anders Levermann (Germany), Mark A. Merrifield (USA), Glenn A. Milne (Canada), R. Steven Nerem (USA), Patrick D. Nunn (Australia), Antony J. Payne (UK), W. Tad Pfeffer (USA), Detlef Stammer (Germany), Alakkat S. Unnikrishnan (India)

Contributing Authors:
David Bahr (USA), Jason E. Box (Denmark/USA), David H. Bromwich (USA), Mark Carson (Germany), William Collins (UK), Xavier Fettweis (Belgium), Piers Forster (UK), Alex Gardner (USA), W. Roland Gehrels (UK), Rianne Giesen (Netherlands), Peter J. Gleckler (USA), Peter Good (UK), Rune Grand Graversen (Sweden), Ralf Greve (Japan), Stephen Griffies (USA), Edward Hanna (UK), Mark Hemer (Australia), Regine Hock (USA), Simon J. Holgate (UK), John Hunter (Australia), Philippe Huybrechts (Belgium), Gregory Johnson (USA), Ian Joughin (USA), Georg Kaser (Austria), Caroline Katsman (Netherlands), Leonard Konikow (USA), Gerhard Krinner (France), Anne Le Brocq (UK), Jan Lenaerts (Netherlands), Stefan Ligtenberg (Netherlands), Christopher M. Little (USA), Ben Marzeion (Austria), Kathleen L. McInnes (Australia), Sebastian H. Mernild (USA), Didier Monselesan (Australia), Ruth Mottram (Denmark), Tavi Murray (UK), Gunnar Myhre (Norway), J.P. Nicholas (USA), Faezeh Nick (Norway), Mahé Perrette (Germany), David Pollard (USA), Valentina Radić (Canada), Jamie Rae (UK), Markku Rummukainen (Sweden), Christian Schoof (Canada), Aimée Slangen (Australia/Netherlands), Jan H. van Angelen (Netherlands), Willem Jan van de Berg (Netherlands), Michiel van den Broeke (Netherlands), Miren Vizcaíno (Netherlands), Yoshihide Wada (Netherlands), Neil J. White (Australia), Ricarda Winkelmann (Germany), Jianjun Yin (USA), Masakazu Yoshimori (Japan), Kirsten Zickfeld (Canada)

Review Editors:
Jean Jouzel (France), Roderik van de Wal (Netherlands), Philip L. Woodworth (UK), Cunde Xiao (China)

This chapter should be cited as:
Church, J.A., P.U. Clark, A. Cazenave, J.M. Gregory, S. Jevrejeva, A. Levermann, M.A. Merrifield, G.A. Milne, R.S. Nerem, P.D. Nunn, A.J. Payne, W.T. Pfeffer, D. Stammer and A.S. Unnikrishnan, 2013: Sea Level Change. In: *Climate Change 2013: The Physical Science Basis. Contribution of Working Group I to the Fifth Assessment Report of the Intergovernmental Panel on Climate Change* [Stocker, T.F., D. Qin, G.-K. Plattner, M. Tignor, S.K. Allen, J. Boschung, A. Nauels, Y. Xia, V. Bex and P.M. Midgley (eds.)]. Cambridge University Press, Cambridge, United Kingdom and New York, NY, USA.

5 horizontaal

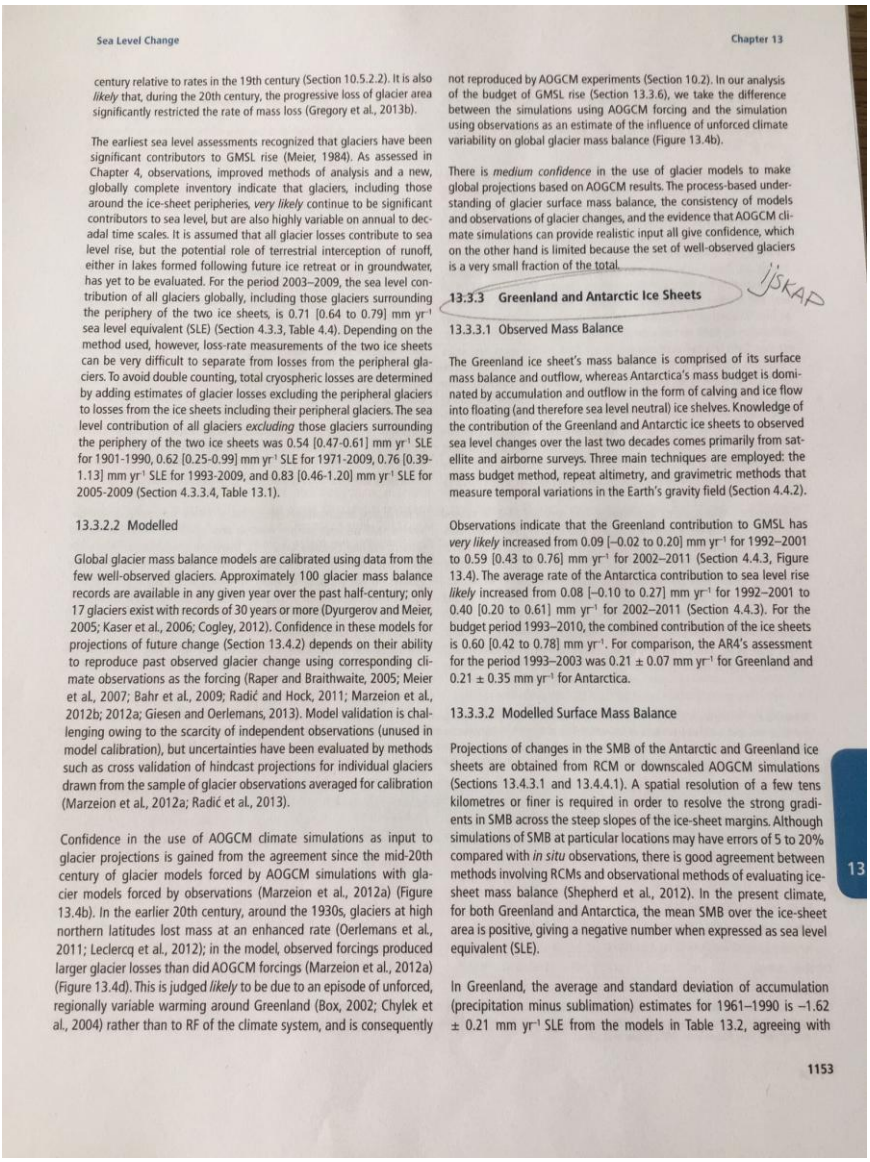

century relative to rates in the 19th century (Section 10.5.2.2). It is also *likely* that, during the 20th century, the progressive loss of glacier area significantly restricted the rate of mass loss (Gregory et al., 2013b).

The earliest sea level assessments recognized that glaciers have been significant contributors to GMSL rise (Meier, 1984). As assessed in Chapter 4, observations, improved methods of analysis and a new, globally complete inventory indicate that glaciers, including those around the ice-sheet peripheries, *very likely* continue to be significant contributors to sea level, but are also highly variable on annual to decadal time scales. It is assumed that all glacier losses contribute to sea level rise, but the potential role of terrestrial interception of runoff, either in lakes formed following future ice retreat or in groundwater, has yet to be evaluated. For the period 2003–2009, the sea level contribution of all glaciers globally, including those glaciers surrounding the periphery of the two ice sheets, is 0.71 [0.64 to 0.79] mm yr^{-1} sea level equivalent (SLE) (Section 4.3.3, Table 4.4). Depending on the method used, however, loss-rate measurements of the two ice sheets can be very difficult to separate from losses from the peripheral glaciers. To avoid double counting, total cryospheric losses are determined by adding estimates of glacier losses excluding the peripheral glaciers to losses from the ice sheets including their peripheral glaciers. The sea level contribution of all glaciers *excluding* those glaciers surrounding the periphery of the two ice sheets was 0.54 [0.47-0.61] mm yr^{-1} SLE for 1901-1990, 0.62 [0.25-0.99] mm yr^{-1} SLE for 1971-2009, 0.76 [0.39-1.13] mm yr^{-1} SLE for 1993-2009, and 0.83 [0.46-1.20] mm yr^{-1} SLE for 2005-2009 (Section 4.3.3.4, Table 13.1).

13.3.2.2 Modelled

Global glacier mass balance models are calibrated using data from the few well-observed glaciers. Approximately 100 glacier mass balance records are available in any given year over the past half-century; only 17 glaciers exist with records of 30 years or more (Dyurgerov and Meier, 2005; Kaser et al., 2006; Cogley, 2012). Confidence in these models for projections of future change (Section 13.4.2) depends on their ability to reproduce past observed glacier change using corresponding climate observations as the forcing (Raper and Braithwaite, 2005; Meier et al., 2007; Bahr et al., 2009; Radić and Hock, 2011; Marzeion et al., 2012b; 2012a; Giesen and Oerlemans, 2013). Model validation is challenging owing to the scarcity of independent observations (unused in model calibration), but uncertainties have been evaluated by methods such as cross validation of hindcast projections for individual glaciers drawn from the sample of glacier observations averaged for calibration (Marzeion et al., 2012a; Radić et al., 2013).

Confidence in the use of AOGCM climate simulations as input to glacier projections is gained from the agreement since the mid-20th century of glacier models forced by AOGCM simulations with glacier models forced by observations (Marzeion et al., 2012a) (Figure 13.4b). In the earlier 20th century, around the 1930s, glaciers at high northern latitudes lost mass at an enhanced rate (Oerlemans et al., 2011; Leclercq et al., 2012); in the model, observed forcings produced larger glacier losses than did AOGCM forcings (Marzeion et al., 2012a) (Figure 13.4d). This is judged *likely* to be due to an episode of unforced, regionally variable warming around Greenland (Box, 2002; Chylek et al., 2004) rather than to RF of the climate system, and is consequently not reproduced by AOGCM experiments (Section 10.2). In our analysis of the budget of GMSL rise (Section 13.3.6), we take the difference between the simulations using AOGCM forcing and the simulation using observations as an estimate of the influence of unforced climate variability on global glacier mass balance (Figure 13.4b).

There is *medium confidence* in the use of glacier models to make global projections based on AOGCM results. The process-based understanding of glacier surface mass balance, the consistency of models and observations of glacier changes, and the evidence that AOGCM climate simulations can provide realistic input all give confidence, which on the other hand is limited because the set of well-observed glaciers is a very small fraction of the total.

13.3.3 Greenland and Antarctic Ice Sheets

13.3.3.1 Observed Mass Balance

The Greenland ice sheet's mass balance is comprised of its surface mass balance and outflow, whereas Antarctica's mass budget is dominated by accumulation and outflow in the form of calving and ice flow into floating (and therefore sea level neutral) ice shelves. Knowledge of the contribution of the Greenland and Antarctic ice sheets to observed sea level changes over the last two decades comes primarily from satellite and airborne surveys. Three main techniques are employed: the mass budget method, repeat altimetry, and gravimetric methods that measure temporal variations in the Earth's gravity field (Section 4.4.2).

Observations indicate that the Greenland contribution to GMSL has *very likely* increased from 0.09 [–0.02 to 0.20] mm yr^{-1} for 1992–2001 to 0.59 [0.43 to 0.76] mm yr^{-1} for 2002–2011 (Section 4.4.3, Figure 13.4). The average rate of the Antarctica contribution to sea level rise *likely* increased from 0.08 [–0.10 to 0.27] mm yr^{-1} for 1992–2001 to 0.40 [0.20 to 0.61] mm yr^{-1} for 2002–2011 (Section 4.4.3). For the budget period 1993–2010, the combined contribution of the ice sheets is 0.60 [0.42 to 0.78] mm yr^{-1}. For comparison, the AR4's assessment for the period 1993–2003 was 0.21 ± 0.07 mm yr^{-1} for Greenland and 0.21 ± 0.35 mm yr^{-1} for Antarctica.

13.3.3.2 Modelled Surface Mass Balance

Projections of changes in the SMB of the Antarctic and Greenland ice sheets are obtained from RCM or downscaled AOGCM simulations (Sections 13.4.3.1 and 13.4.4.1). A spatial resolution of a few tens kilometres or finer is required in order to resolve the strong gradients in SMB across the steep slopes of the ice-sheet margins. Although simulations of SMB at particular locations may have errors of 5 to 20% compared with *in situ* observations, there is good agreement between methods involving RCMs and observational methods of evaluating ice-sheet mass balance (Shepherd et al., 2012). In the present climate, for both Greenland and Antarctica, the mean SMB over the ice-sheet area is positive, giving a negative number when expressed as sea level equivalent (SLE).

In Greenland, the average and standard deviation of accumulation (precipitation minus sublimation) estimates for 1961–1990 is –1.62 ± 0.21 mm yr^{-1} SLE from the models in Table 13.2, agreeing with

physical detail of its surface scheme, MAR is considered the most realistic model, and yields a threshold value 2.8 [2.1 to 3.4] °C for changes in Greenland annual average temperature compared to pre-industrial. Using MAR driven with output from various CMIP5 AOGCMs, Fettweis et al. (2013) evaluated the threshold as ~3°C in GMST above 1980–1999 (hence about 3.5°C relative to pre-industrial), and found that it is not exceeded in the 21st century under the RCP4.5 scenario but is reached around 2070 under the RCP8.5 scenario.

Some of the uncertainty in the threshold results from the value assumed for the steady state ice-sheet SMB (see Table 13.2), and whether this is assumed to be pre-industrial or a more recent period. For 400 Gt yr^{-1} (Fettweis et al., 2013), the parametrization of Greenland ice sheet SMB used for present assessment of 21st century changes (Section 13.4.3.1, Supplementary Material) gives a global warming threshold of 3.0 [2.1 to 4.1] °C with respect to 1860–1879 (the reference period used in Box 13.1); for 225 Gt yr^{-1} (Gregory and Huybrechts, 2006, following Church et al., 2001), the threshold is 2.1 [1.5 to 3.0] °C.

Although a negative SMB is a sufficient condition for passing the threshold, it will overestimate the value of the threshold quantitatively, because the SMB–height feedback (even without passing the threshold) means that the steady-state SMB is reduced by more than is calculated assuming fixed topography. The actual SMB change will depend on the dynamical response of the ice sheet that determines its topography. Constraining simulations with a dynamic ice-sheet model to changes during the last interglacial, Robinson et al. (2012) estimated the threshold as 1.6 [0.9 to 2.8] °C global averaged temperature above pre-industrial. In these simulations, they find that the threshold is passed when southeastern Greenland has a negative SMB. The near-complete ice loss then occurs through ice flow and SMB.

The complete loss of the ice sheet is not inevitable because it has a long time scale (tens of millennia near the threshold and a millennium or more for temperatures a few degrees above the threshold). If the surrounding temperatures decline before the ice sheet is eliminated, the ice sheet might regrow. In the context of future GHG emissions, the time scale of ice loss is competing with the time scale of temperature decline after a reduction of GHG emissions (Allen et al., 2009; Solomon et al., 2009; Zickfeld et al., 2009). The outcome therefore depends on both the CO_2 concentration and on how long it is sustained. Charbit et al. (2008) found that loss of the ice sheet is inevitable for cumulative emissions above about 3000 GtC, but a partial loss followed by regrowth occurs for cumulative emissions less than 2500 GtC. Ridley et al. (2010) identified three steady states of the ice sheet. If the CO_2 concentration is returned to pre-industrial when more than 20 to 40% of the ice sheet has been lost, it will regrow only to 80% of its original volume due to a local climate feedback in one region; if 50% or more, it regrows to 20 to 40% of the original. Similar states with ice volume around 20%, 60 to 80% and 100% of the initial ice volume are also found in other models (Langen et al., 2012; Robinson et al., 2012). If all the ice is lost, temperatures must decline to below a critical threshold for regrowth of the ice sheet (Robinson et al., 2012; Solgaard and Langen, 2012).

On the evidence of paleo data and modelling (Section 5.6.2.3, 13.2.1), it is *likely* that during the LIG, when global mean temperature never exceeded 2°C pre-industrial, the Greenland ice sheet contributed no more than ~4 m to GMSL. This could indicate that the threshold for near-complete deglaciation had not been passed, or that it was not greatly exceeded so that the rate of mass loss was low; however, the forcing responsible for the LIG warming was orbital rather than from CO_2 (van de Berg et al., 2011), so it is not a direct analogue and the applicable threshold may be different. Studies with fixed-topography ice sheets indicate a threshold of 2°C or above of global warming with respect to pre-industrial for near-complete loss of the Greenland ice sheet, while the one study (and therefore *low confidence*) presently available with a dynamical ice sheet suggests that the threshold could be as low as about 1°C (Robinson et al. 2012). Recent studies with fixed-topography ice sheets indicate that the threshold is less than about 4°C (*medium confidence* because of multiple studies). With currently available information, we do not have sufficient confidence to assign a *likely* range for the threshold. If the threshold is exceeded temporarily, an irreversible loss of part or most of the Greenland ice sheet could result, depending on the duration and amount that the threshold is exceeded.

13.4.4 Antarctic Ice Sheet

13.4.4.1 Surface Mass Balance Change

Because the ice loss from Antarctica due to surface melt and runoff is about 1% of the total mass gain from snowfall, most ice loss occurs through solid ice discharge into the ocean. In the 21st century, ablation is projected to remain small on the Antarctic ice sheet because low surface temperatures inhibit surface melting, except near the coast and on the Antarctic Peninsula, and meltwater and rain continue to freeze in the snowpack (Ligtenberg et al., 2013). Projections of Antarctic SMB changes over the 21st century thus indicate a negative contribution to sea level because of the projected widespread increase in snowfall associated with warming air temperatures (Krinner et al., 2007; Uotila et al., 2007; Bracegirdle et al., 2008). Several studies (Krinner et al., 2007; Uotila et al., 2007; Bengtsson et al., 2011) have shown that the precipitation increase is directly linked to atmospheric warming via the increased moisture holding capacity of warmer air, and is therefore larger for scenarios of greater warming. The relationship is exponential, resulting in an increase of SMB as a function of Antarctic SAT change evaluated in various recent studies with high-resolution (~60 km) models as 3.7% $°C^{-1}$ (Bengtsson et al., 2011), 4.8% $°C^{-1}$ (Ligtenberg et al., 2013) and ~7% $°C^{-1}$ (Krinner et al., 2007). These agree well with the sensitivity of 5.1 ± 1.5% $°C^{-1}$ (one standard deviation) of CMIP3 AOGCMs (Gregory and Huybrechts, 2006).

The effect of atmospheric circulation changes on continental-mean SMB is an order of magnitude smaller than the effect of warming, but circulation changes can have a large influence on regional changes in accumulation, particularly near the ice-sheet margins (Uotila et al., 2007) where increased accumulation may induce additional ice flow across the grounding line (Huybrechts and De Wolde, 1999; Gregory and Huybrechts, 2006; Winkelmann et al., 2012). Simulated SMB is strongly and nonlinearly influenced by ocean surface temperature and sea-ice conditions (Swingedouw et al., 2008). This dependence means that the biases in the model-control climate may distort the SMB sensitivity to climate change, suggesting that more accurate predictions

8 horizontaal

that the long-term trend estimate in GMSL is 1.7 [1.5 to 1.9] mm yr^{-1} between 1901 and 2010 for a total sea level rise of 0.19 [0.17 to 0.21] m (Figure 13.3c). Interannual and decadal-scale variability is superimposed on the long-term MSL trend, and Chapter 3 noted that discrepancies between the various published MSL records are present at these shorter time scales.

Section 3.7 also concludes that it is *likely* that the rate of sea level rise increased from the 19th century to the 20th century. Taking this evidence in conjunction with the proxy evidence for a change of rate (Sections 5.6.3 and 13.2.1; Figure 13.3b), there is *high confidence* that the rate of sea level rise has increased during the last two centuries, and it is *likely* that GMSL has accelerated since the early 1900's. Because of the presence of low-frequency variations (e.g., multi-decadal variations seen in some tide gauge records; Chambers et al. (2012)), sea level acceleration results are sensitive to the choice of the analysis time span. When a 60-year oscillation is modelled along with an acceleration term, the estimated acceleration in GMSL (twice the quadratic term) computed over 1900–2010 ranges from 0.000 [–0.002 to 0.002] mm yr^{-2} in the Ray and Douglas (2011) record, to 0.013 [0.007 to 0.019] mm yr^{-2} in the Jevrejeva et al. (2008) record, and 0.012 [0.009 to 0.015] mm yr^{-2} in the Church and White (2011) record. For comparison, Church and White (2011) estimated the acceleration term to be 0.009 [0.004 to 0.014] mm yr^{-2} over the 1880–2009 time span when the 60-year cycle is not considered.

13.2.2.2 The Satellite Altimeter Record (1993–2012)

The high-precision satellite altimetry record started in 1992 and provides nearly global (±66°) sea level measurements at 10-day intervals. Ollivier et al. (2012) showed that Envisat, which observes to ±82° latitude, provides comparable GMSL estimates. Although there are slight differences at interannual time scales in the altimetry-based GMSL time series produced by different groups (Masters et al., 2012), there is very good agreement on the 20-year long GMSL trend (Figure 13.3d). After accounting for the ~ –0.3 mm yr^{-1} correction related to the increasing size of the global ocean basins due to GIA (Peltier, 2009), a GMSL rate of 3.2 [2.8 to 3.6] mm yr^{-1} over 1993–2012 is found by the different altimetry data processing groups. The current level of precision is derived from assessments of all source of errors affecting the altimetric measurements (Ablain et al., 2009) and from tide gauge comparisons (Beckley et al., 2010; Nerem et al., 2010). Chapter 3 concludes that the GMSL trend since 1993 is *very likely* higher compared to the mean rates over the 20th century, and that it is *likely* that GMSL rose between 1920 and 1950 at a rate comparable to that observed since 1993. This recent higher rate is also seen in tide gauge data over the same period, but on the basis of observations alone it does not necessarily reflect a recent acceleration, considering the previously reported multi-decadal variations of mean sea level. The rapid increase in GMSL since 2011 is related to the recovery from the 2011 La Niña event (Section 13.3.5) (Boening et al., 2012).

13.3 Contributions to Global Mean Sea Level Rise During the Instrumental Period

In order to assess our understanding of the causes of observed changes and our confidence in projecting future changes we compare observational estimates of contributions with results derived from AOGCM experiments, beginning in the late 19th century, forced with estimated past time-dependent anthropogenic changes in atmospheric composition and natural forcings due to volcanic aerosols and variations in solar irradiance (Section 10.1). This period and these simulations are often referred to as "historical."

13.3.1 Thermal Expansion Contribution

13.3.1.1 Observed

Important progress has been realized since AR4 in quantifying the observed thermal expansion component of global mean sea level rise. This progress reflects (1) the detection of systematic time-dependent depth biases affecting historical expendable bathythermograph data (Gouretski and Koltermann, 2007) (Chapter 3), (2) the newly available Argo Project ocean (temperature and salinity) data with almost global coverage (not including ice-covered regions and marginal seas) of the oceans down to 2000 m since 2004–2005, and (3) estimates of the deep-ocean contribution using ship-based data collected during the World Ocean Circulation Experiment and revisit cruises (Johnson and Gruber, 2007; Johnson et al., 2007; Purkey and Johnson, 2010; Kouketsu et al., 2011).

For the period 1971–2010, the rate for the 0 to 700 m depth range is 0.6 [0.4 to 0.8] mm yr^{-1} (Section 3.7.2 and Table 3.1). Including the deep-ocean contribution for the same period increases the value to 0.8 [0.5 to 1.1] mm yr^{-1} (Table 13.1). Over the altimetry period (1993–2010), the rate for the 0 to 700 m depth range is 0.8 [0.5 to 1.1] mm yr^{-1} and 1.1 [0.8 to 1.4] mm yr^{-1} when accounting for the deep ocean (Section 3.7.2, Table 3.1, Table 13.1).

13.3.1.2 Modelled

GMSL rise due to thermal expansion is approximately proportional to the increase in ocean heat content (Section 13.4.1). Historical GMSL rise due to thermal expansion simulated by CMIP5 models is shown in Table 13.1 and Figure 13.4a. The model spread is due to uncertainty in RF and modelled climate response (Sections 8.5.2, 9.4.2.2, 9.7.2.5 and 13.4.1).

In the time mean of several decades, there is a negative volcanic forcing if there is more volcanic activity than is typical of the long term, and a positive forcing if there is less. In the decades after major volcanic eruptions, the rate of expansion is temporarily enhanced, as the ocean recovers from the cooling caused by the volcanic forcing (Church et al., 2005; Gregory et al., 2006) (Figure 13.4a). During 1961–1999, a period when there were several large volcanic eruptions, the CMIP3 simulations with both natural and anthropogenic forcing have substantially smaller increasing trends in the upper 700 m than those with anthropogenic forcing only (Domingues et al., 2008) because the natural volcanic forcing tends to cool the climate system, thus reducing ocean

10 horizontaal

Table 13.1 | Global mean sea level budget (mm yr^{-1}) over different time intervals from observations and from model-based contributions. Uncertainties are 5 to 95%. The Atmosphere–Ocean General Circulation Model (AOGCM) historical integrations end in 2005; projections for RCP4.5 are used for 2006–2010. The modelled thermal expansion and glacier contributions are computed from the CMIP5 results, using the model of Marzeion et al. (2012a) for glaciers. The land water contribution is due to anthropogenic intervention only, not including climate-related fluctuations.

Source	1901–1990	1971–2010	1993–2010
Observed contributions to global mean sea level (GMSL) rise			
Thermal expansion	–	0.8 [0.5 to 1.1]	1.1 [0.8 to 1.4]
Glaciers except in Greenland and Antarctica[a]	0.54 [0.47 to 0.61]	0.62 [0.25 to 0.99]	0.76 [0.39 to 1.13]
Glaciers in Greenland[a]	0.15 [0.10 to 0.19]	0.06 [0.03 to 0.09]	0.10 [0.07 to 0.13][b]
Greenland ice sheet	–	–	0.33 [0.25 to 0.41]
Antarctic ice sheet	–	–	0.27 [0.16 to 0.38]
Land water storage	−0.11 [−0.16 to −0.06]	0.12 [0.03 to 0.22]	0.38 [0.26 to 0.49]
Total of contributions	–	–	**2.8 [2.3 to 3.4]**
Observed GMSL rise	**1.5 [1.3 to 1.7]**	**2.0 [1.7 to 2.3]**	**3.2 [2.8 to 3.6]**
Modelled contributions to GMSL rise			
Thermal expansion	0.37 [0.06 to 0.67]	0.96 [0.51 to 1.41]	1.49 [0.97 to 2.02]
Glaciers except in Greenland and Antarctica	0.63 [0.37 to 0.89]	0.62 [0.41 to 0.84]	0.78 [0.43 to 1.13]
Glaciers in Greenland	0.07 [−0.02 to 0.16]	0.10 [0.05 to 0.15]	0.14 [0.06 to 0.23]
Total including land water storage	**1.0 [0.5 to 1.4]**	**1.8 [1.3 to 2.3]**	**2.8 [2.1 to 3.5]**
Residual[c]	**0.5 [0.1 to 1.0]**	**0.2 [−0.4 to 0.8]**	**0.4 [−0.4 to 1.2]**

Notes:
[a] Data for all glaciers extend to 2009, not 2010.
[b] This contribution is not included in the total because glaciers in Greenland are included in the observational assessment of the Greenland ice sheet.
[c] Observed GMSL rise – modelled thermal expansion – modelled glaciers – observed land water storage.

heat uptake (Levitus et al., 2001). The models including natural forcing are closer to observations, though with a tendency to underestimate the trend by about 10% (Sections 9.4.2.2 and 10.4.1).

Gregory (2010) and Gregory et al. (2013a) proposed that AOGCMs underestimate ocean heat uptake in their historical simulations because their control experiments usually omit volcanic forcing, so the imposition of historical volcanic forcing on the simulated climate system represents a time mean negative forcing relative to the control climate. The apparent long persistence of the simulated oceanic cooling following the 1883 eruption of Krakatau (Delworth et al., 2005; Gleckler et al., 2006a, 2006b; Gregory et al., 2006) is a consequence of this bias, which also causes a model-dependent underestimate of up to 0.2 mm yr^{-1} of thermal expansion on average during the 20th century (Gregory et al., 2013a, 2013b). This implies that CMIP5 results may be similarly underestimated, depending on the details of the individual model control runs. Church et al. (2013) proposed a correction of 0.1 mm yr^{-1} to the model mean rate, which we apply in the sea level budget in Table 13.1 and Figure 13.7. The corrected CMIP5 model mean rate for 1971–2010 is close to the central observational estimate; the model mean rate for 1993–2010 exceeds the central observational estimate but they are not statistically different given the uncertainties (Table 13.1 and Figure 13.4a). This correction is not made to projections of thermal expansion because it is very small compared with the projected increase in the rate (Section 13.5.1).

In view of the improvement in observational estimates of thermal expansion, the good agreement of historical model results with observational estimates, and their consistency with understanding of the energy budget and RF of the climate system (Box 13.1), we have *high confidence* in the projections of thermal expansion using AOGCMs.

13.3.2 Glaciers

13.3.2.1 Observed

'Glaciers' are defined here as all land-ice masses, including those peripheral to (but not including) the Greenland and Antarctic ice sheets. The term 'glaciers and ice caps' was applied to this category in the AR4. Changes in aggregate glacier volume have conventionally been determined by various methods of repeat mapping of surface elevation to detect elevation (and thus volume) change. Mass changes are determined by compilation and upscaling of limited direct observations of surface mass balance (SMB). Since 2003, gravity observations from Gravity Recovery and Climate Experiment (GRACE) satellites have been used to detect mass change of the world's glaciers.

The combined records indicate that a net decline of global glacier volume began in the 19th century, before significant anthropogenic RF had started, and was probably the result of warming associated with the termination of the Little Ice Age (Crowley, 2000; Gregory et al., 2006, 2013b). Global rates of glacier volume loss did not increase significantly during much of the 20th century (Figure 4.12). In part this may have been because of an enhanced rate of loss due to unforced high-latitude variability early in the century, while anthropogenic warming was still comparatively small (Section 13.3.2.2). It is *likely* that anthropogenic forcing played a statistically significant role in acceleration of global glacier losses in the latter decades of the 20th

11 horizontaal

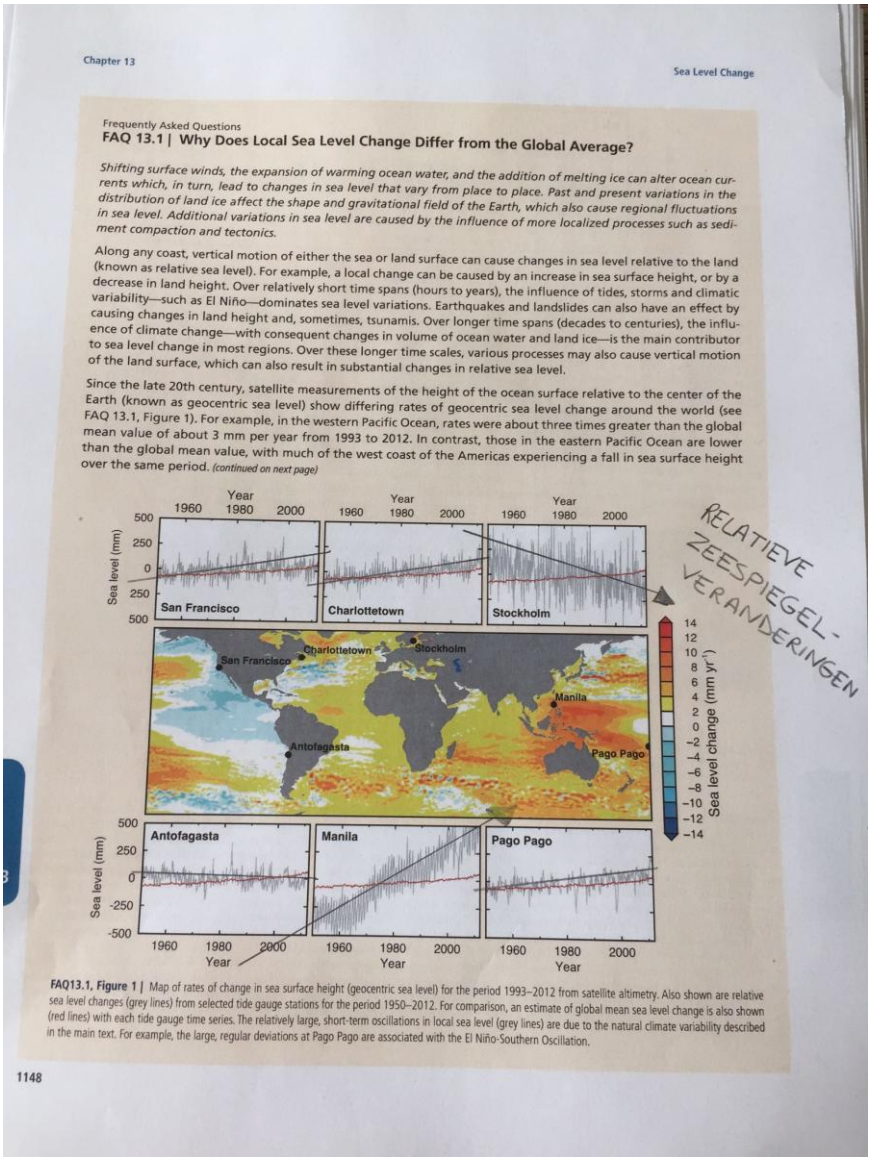

Frequently Asked Questions

FAQ 13.1 | Why Does Local Sea Level Change Differ from the Global Average?

Shifting surface winds, the expansion of warming ocean water, and the addition of melting ice can alter ocean currents which, in turn, lead to changes in sea level that vary from place to place. Past and present variations in the distribution of land ice affect the shape and gravitational field of the Earth, which also cause regional fluctuations in sea level. Additional variations in sea level are caused by the influence of more localized processes such as sediment compaction and tectonics.

Along any coast, vertical motion of either the sea or land surface can cause changes in sea level relative to the land (known as relative sea level). For example, a local change can be caused by an increase in sea surface height, or by a decrease in land height. Over relatively short time spans (hours to years), the influence of tides, storms and climatic variability—such as El Niño—dominates sea level variations. Earthquakes and landslides can also have an effect by causing changes in land height and, sometimes, tsunamis. Over longer time spans (decades to centuries), the influence of climate change—with consequent changes in volume of ocean water and land ice—is the main contributor to sea level change in most regions. Over these longer time scales, various processes may also cause vertical motion of the land surface, which can also result in substantial changes in relative sea level.

Since the late 20th century, satellite measurements of the height of the ocean surface relative to the center of the Earth (known as geocentric sea level) show differing rates of geocentric sea level change around the world (see FAQ 13.1, Figure 1). For example, in the western Pacific Ocean, rates were about three times greater than the global mean value of about 3 mm per year from 1993 to 2012. In contrast, those in the eastern Pacific Ocean are lower than the global mean value, with much of the west coast of the Americas experiencing a fall in sea surface height over the same period. *(continued on next page)*

RELATIEVE ZEESPIEGEL-VERANDERINGEN

FAQ13.1, Figure 1 | Map of rates of change in sea surface height (geocentric sea level) for the period 1993–2012 from satellite altimetry. Also shown are relative sea level changes (grey lines) from selected tide gauge stations for the period 1950–2012. For comparison, an estimate of global mean sea level change is also shown (red lines) with each tide gauge time series. The relatively large, short-term oscillations in local sea level (grey lines) are due to the natural climate variability described in the main text. For example, the large, regular deviations at Pago Pago are associated with the El Niño-Southern Oscillation.

2 verticaal

Geen specifieke hint behalve idem als 1 horizontaal.

3 verticaal

(Pollard and DeConto, 2009; Hill et al., 2010; Dolan et al., 2011). The assessment by Chapter 5 suggests that GMSL was above present, but that it did not exceed 20 m above present, during the middle Pliocene warm periods (*high confidence*).

13.2.1.2 Marine Isotope Stage 11

During marine isotope stage 11 (MIS 11; 401 to 411 ka), Antarctic ice core and tropical Pacific paleo temperature estimates suggest that global temperature was 1.5°C to 2.0°C warmer than pre-industrial (*low confidence*) (Masson-Delmotte et al., 2010). Studies of the magnitude of sea level highstands from raised shorelines attributed to MIS 11 have generated highly divergent estimates. Since the AR4, studies have accounted for GIA effects (Raymo and Mitrovica, 2012) or reported elevations from sites where the GIA effects are estimated to be small (Muhs et al., 2012; Roberts et al., 2012). From this evidence, our assessment is that MIS 11 GMSL reached 6 to 15 m higher than present (*medium confidence*), requiring a loss of most or all of the present Greenland ice sheet and WAIS plus a reduction in the EAIS of up to 5 m equivalent sea level if sea level rise was at the higher end of the range.

13.2.1.3 The Last Interglacial Period

New data syntheses and model simulations since the AR4 indicate that during the Last Interglacial Period (LIG, ~129 to 116 ka), global mean annual temperature was 1°C to 2°C warmer than pre-industrial (*medium confidence*) with peak global annual sea surface temperatures (SSTs) that were 0.7°C ± 0.6°C warmer (*medium confidence*) (Section 5.3.4). High latitude surface temperature, averaged over several thousand years, was at least 2°C warmer than present (*high confidence*) (Section 5.3.4). There is robust evidence and high agreement that under the different orbital forcing and warmer climate of the LIG, sea level was higher than present. There have been a large number of estimates of the magnitude of LIG GMSL rise from localities around the globe, but they are generally from a small number of RSL reconstructions, and do not consider GIA effects, which can be substantial (Section 5.6.2). Since the AR4, two approaches have addressed GIA effects in order to infer LIG sea level from RSL observations at coastal sites. Kopp et al. (2009, 2013) obtained a probabilistic estimate of GMSL based on a large and geographically broadly distributed database of LIG sea level indicators. Their analysis accounted for GIA effects (and their uncertainties) as well as uncertainties in geochronology, the interpretation of sea level indicators, and regional tectonic uplift and subsidence. Kopp et al. (2013) concluded that GMSL was 6.4 m (95% probability) and 7.7 m (67% probability) higher than present, and with a 33% probability that it exceeded 8.8 m. The other approach, taken by Dutton and Lambeck (2012), used data from far-field sites that are tectonically stable. Their estimate of 5.5 to 9 m LIG GMSL is consistent with the probabilistic estimates made by Kopp et al. (2009, 2013). Chapter 5 thus concluded there is *very high confidence* that the maximum GMSL during the LIG was at least 5 m higher than present and *high confidence* it did not exceed 10 m. The best estimate is 6 m higher than present. Chapter 5 also concluded from ice-sheet model simulations and elevation changes derived from a new Greenland ice core that the Greenland ice sheet *very likely* contributed between 1.4 and 4.3 m sea level equivalent. This implies with *medium confidence* a contribution from the Antarctic ice sheet to the global mean sea level during the last interglacial period, but this is not yet supported by observational and model evidence.

There is *medium confidence* for a sea level fluctuation of up to 4 m during the LIG, but regional sea level variability and uncertainties in sea level proxies and their ages cause differences in the timing and amplitude of the reported fluctuation (Kopp et al., 2009, 2013; Thompson et al., 2011). For the time interval during the LIG in which GMSL was above present, there is *high confidence* that the maximum 1000-year average rate of GMSL rise associated with the sea level fluctuation exceeded 2 m kyr^{-1} but that it did not exceed 7 m kyr^{-1} (Chapter 5) (Kopp et al., 2013). Faster rates lasting less than a millennium cannot be ruled out by these data. Therefore, there is *high confidence* that there were intervals when rates of GMSL rise during the LIG exceeded the 20th century rate of 1.7 [1.5 to 1.9] mm yr^{-1}.

13.2.1.4 The Late Holocene

Since the AR4, there has been significant progress in resolving the sea level history of the last 7000 years. RSL records indicate that from ~7 to 3 ka, GMSL *likely* rose 2 to 3 m to near present-day levels (Chapter 5). Based on local sea level records spanning the last 2000 years, there is *medium confidence* that fluctuations in GMSL during this interval have not exceeded ~ ±0.25 m on time scales of a few hundred years (Section 5.6.3, Figure 13.3a). The most robust signal captured in salt marsh records from both Northern and Southern Hemispheres supports the AR4 conclusion for a transition from relatively low rates of change during the late Holocene (order tenths of mm yr^{-1}) to modern rates (order mm yr^{-1}) (Section 5.6.3, Figure 13.3b). However, there is variability in the magnitude and the timing (1840–1920) of this increase in both paleo and instrumental (tide gauge) records (Section 3.7). By combining paleo sea level records with tide gauge records at the same localities, Gehrels and Woodworth (2013) concluded that sea level began to rise above the late Holocene background rate between 1905 and 1945, consistent with the conclusions by Lambeck et al. (2004).

13.2.2 The Instrumental Record (~1700–2012)

The instrumental record of sea level change is mainly comprised of tide gauge measurements over the past two to three centuries (Figures 13.3b and 13.3c) and, since the early 1990s, of satellite-based radar altimeter measurements (Figure 13.3d).

13.2.2.1 The Tide Gauge Record (~1700–2012)

= GETIJMETER

The number of tide gauges has increased since the first gauges at some northern European ports were installed in the 18th century; Southern Hemisphere (SH) measurements started only in the late 19th century. Section 3.7 assesses 20th century sea level rise estimates from tide gauges (Douglas, 2001; Church and White, 2006, 2011; Jevrejeva et al., 2006, 2008; Holgate, 2007; Ray and Douglas, 2011), and concludes that even though different strategies were developed to account for inhomogeneous tide gauge data coverage in space and time, and to correct for vertical crustal motions (also sensed by tide gauges, in addition to sea level change and variability), it is *very likely*

4 verticaal

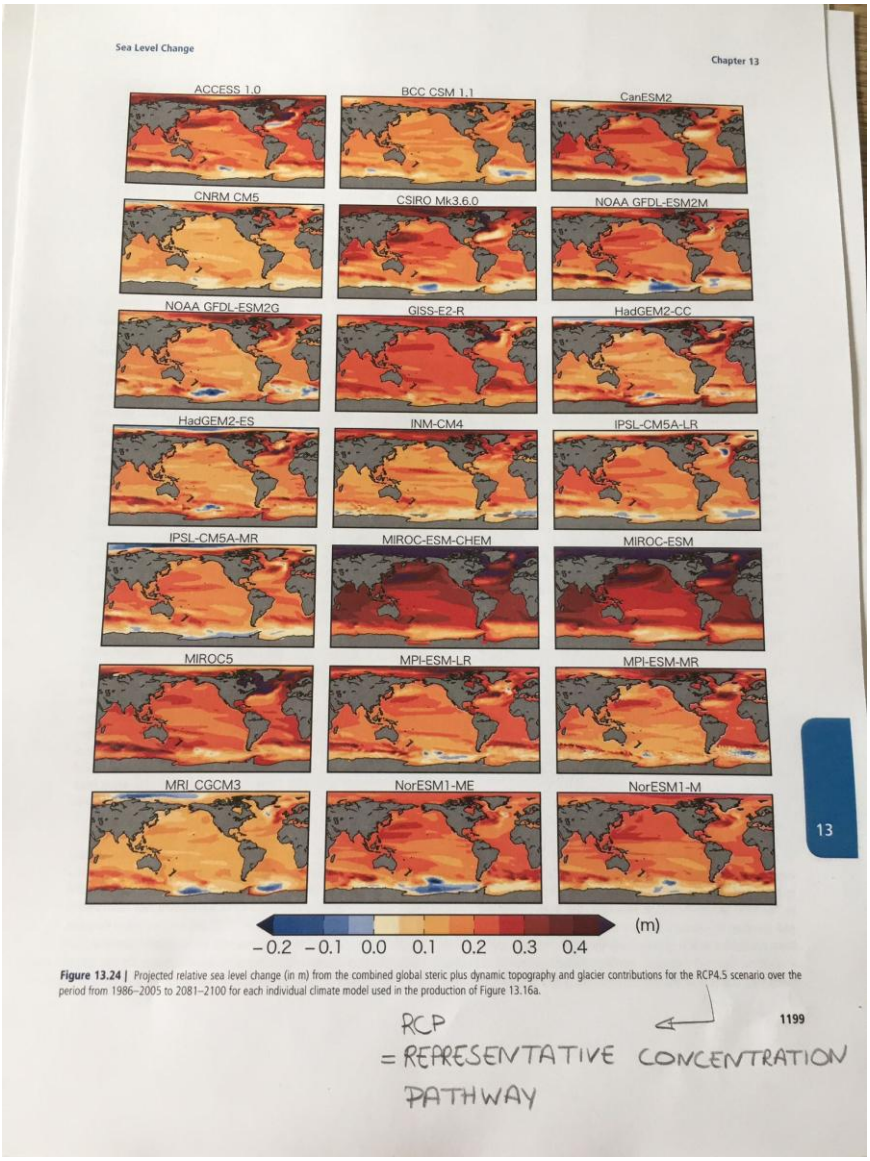

Figure 13.24 | Projected relative sea level change (in m) from the combined global steric plus dynamic topography and glacier contributions for the RCP4.5 scenario over the period from 1986–2005 to 2081–2100 for each individual climate model used in the production of Figure 13.16a.

1199

RCP
= REPRESENTATIVE CONCENTRATION PATHWAY

6 verticaal
Idem aan 11 horizontaal.

7 verticaal

Box 13.2 | History of the Marine Ice-Sheet Instability Hypothesis

Marine ice sheets rest on bedrock that is submerged below sea level (often by 2 to 3 km). The most well-researched marine ice sheet is the West Antarctic ice sheet (WAIS) where approximately 75% of the ice sheet's area currently rests on bedrock below sea level. The East Antarctic ice sheet (EAIS), however, also has appreciable areas grounded below sea level (~35%), in particular around the Totten and Cook Glaciers.

These ice sheets are fringed by floating ice shelves, which are fed by flow from grounded ice across a grounding line (GL). The GL is free to migrate both seawards and landwards as a consequence of the local balance between the weight of ice and displaced ocean water. Depending on a number of factors, which include ice-shelf extent and geometry, ice outflow to the ocean generally (but not always) increases with ice thickness at the GL. Accordingly, when the ice sheet rests on a bed that deepens towards the ice-sheet interior (see Box 13.2, Figure 1a), the ice outflow to the ocean will generally increase as the GL retreats. It is this feature that gives rise to the Marine Ice-Sheet Instability (MISI), which states that a GL cannot remain stable on a landward-deepening slope. Even if snow accumulation and outflow were initially in balance (Box 13.2, Figure 1b), natural fluctuations in climate cause the GL to fluctuate slightly (Box 13.2, Figure 1c). In the case of a retreat, the new GL position is then associated with deeper bedrock and thicker ice, so that outflow increases (Box 13.2, Figure 1d). This increased outflow leads to further, self-sustaining retreat until a region of shallower, seaward-sloping bedrock is reached. Stable configurations can therefore exist only where the GL rests on slopes that deepen towards the ocean. A change in climate can therefore potentially force a large-scale retreat of the GL from one bedrock ridge to another further inland. *(continued on next page)*

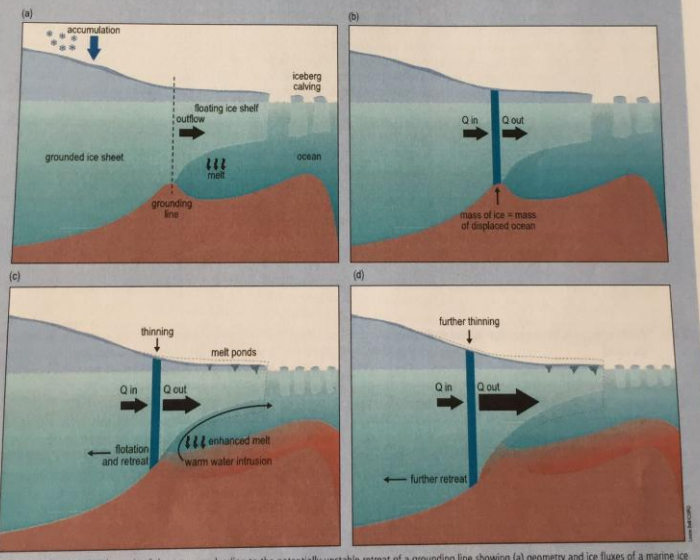

Box 13.2, Figure 1 | Schematic of the processes leading to the potentially unstable retreat of a grounding line showing (a) geometry and ice fluxes of a marine ice sheet, (b) the grounding line in steady state, (c) climate change triggering mass outflow from the ice sheet and the start of grounding line retreat and (d) self-sustained retreat of the grounding line.

13

9 verticaal

13.4.4.2 Dynamical Change

The Antarctic ice sheet represents the largest potential source of future SLR; the West Antarctic ice sheet alone has the potential to raise sea level by ~4.3 m (Fretwell et al., 2013). The rate at which this reservoir will be depleted and cause sea level to rise, however, is not easily quantifiable. In this section, we focus on dynamical changes (i.e., those related to the flow of the ice sheet) that affect SLR by altering the flux of ice across the grounding line (or outflow) that separates ice resting on bedrock (some of which does not currently displace ocean water) from floating ice shelves (which already displace ocean water and have only a negligible effect on sea level) (Jenkins and Holland, 2007).

Issues associated with the inability of models to reproduce recently observed changes in the dynamics of the Antarctic ice sheet prevented the AR4 from quantifying the effect of these changes on future sea level. Since the AR4, progress has been made in understanding the observations (Sections 4.4.3 and 4.4.4), and projections are becoming available. It must be stressed, however, that this field has yet to reach the same level of development that exists for modelling many other components of the Earth system. There is an underlying concern that observations presage the onset of large-scale grounding line retreat in what is termed the Marine Ice Sheet Instability (MISI; Box 13.2), and much of the research assessed here attempts to understand the applicability of this theoretical concept to projected SLR from Antarctica.

There are three distinct processes that could link climate change to dynamical change of the Antarctic ice sheet and potentially trigger increased outflow. These may operate directly through the increased potential for melt ponds to form on the upper surface of ice shelves, which may destabilize them, or by increases in submarine melt experienced by ice shelves as a consequence of oceanic warming, which leads to their thinning, as well as indirectly by coupling between SMB and ice flow. Section 4.4.3.2 presents the observational basis on which understanding of these processes is based, while their potential future importance is assessed here. Literature on the two mechanisms directly linked to climate change will be assessed first, followed by their relation to outflow change and lastly SMB coupling.

IJSPLATEAU

There is strong evidence that regional warming and increased melt water ponding in the Antarctic Peninsula led to the collapse of ice shelves along the length of peninsula (Cook and Vaughan, 2010), most notably the Larsen B ice shelf (MacAyeal et al., 2003). Substantial local warming (~5 to ? °C) would, however, be required before the main Antarctic ice shelves (the Ross and Filchner-Ronne ice shelves) would become threatened (Joughin and Alley, 2011). An assessment of the AR4 AOGCM ensemble under scenario A1B yielded an Antarctic continental-average warming rate of 0.034 ± 0.01°C yr^{-1} (Bracegirdle et al., 2008), suggesting that the required level of warming may not be approached by the end of the 21st century. Using an intermediate complexity model with scenario A2, Fyke et al. (2010) found that melt starts to reach significant levels over these ice shelves around 2100 to 2300. Barrand et al. (2013) made a process-based assessment of the effect of ice-shelf collapse on outflow from the Antarctic Peninsula, which yields a range of SLR at 2100 between 10 and 20 mm, with a bounding maximum of 40 mm.

There is good evidence linking the focus of current Antarctic mass loss in the Amundsen Sea sector of the WAIS (containing Pine Island and Thwaites Glaciers) (Shepherd and Wingham, 2007; Rignot et al., 2008; Pritchard et al., 2009) to the presence of relatively warm Circumpolar Deep Water on the continental shelf (Thoma et al., 2008; Jenkins et al., 2010). However, it is not possible to determine whether this upwelling was related directly or indirectly to a rise in global mean temperature. Yin et al. (2011) assessed output from 19 AOGCMs under scenario A1B to determine how subsurface temperatures are projected to evolve around the West and East Antarctic ice sheets. They showed decadal-mean warming of 0.4°C to 0.7°C and 0.4°C to 0.9°C around West and East Antarctica, respectively (25th to 75th percentiles of ensemble) by the end of the 21st century. More detailed regional modelling using scenario A1B illustrates the potential for warm water to invade the ocean cavity underlying the Filchner-Ronne ice shelf in the second half of the 21st century, with an associated 20-fold increase in melt (Hellmer et al., 2012). Based on the limited literature, there is *medium confidence* that oceanic processes may potentially trigger further dynamical change particularly in the latter part of the 21st century, while there is also *medium confidence* that atmospheric change will not affect dynamics outside of the Antarctic Peninsula during the 21st century.

Several process-based projections of the future evolution of Pine Island Glacier have now been made, and some of the issues that this modelling faced (such as the need for sub-kilometre resolution to ensure consistent results; Cornford et al. (2013), Durand et al. (2009)) are being resolved (Pattyn et al., 2013). In experiments using an idealized increase in marine melt, Joughin et al. (2010) demonstrated only limited (~25 km) retreat of the grounding line before a new equilibrium position was established. Gladstone et al. (2012) used a flowline model forced with ocean-model output (Hellmer et al., 2012) to identify two modes of retreat: one similar to that identified by Joughin et al. (2010), and a second characterized by complete collapse from 2150 onwards. More sophisticated ice-flow modelling (albeit with idealized forcing) suggests grounding line retreat of ~100 km in 50 years (Cornford et al., 2013). These studies support the theoretical finding of Gudmundsson et al. (2012) that grounding line retreat, if triggered, does not inevitably lead to MISI but may halt if local buttressing from ice rises or channel sidewalls is sufficient. Parizek et al. (2013) used a flowline model to study Thwaites Glacier and found that grounding line retreat is possible only under extreme ocean forcing. It is also thought that considerably less back pressure is exerted by Thwaites' ice shelf in comparison to Pine Island's (Rignot, 2001; 2008), which may make it less sensitive to forcing by submarine melt (Schoof, 2007a; Goldberg et al., 2012). Based on this literature, there is *high confidence* that the retreat of Pine Island Glacier (if it occurs) can be characterized by a SLR measured in centimetres by 2100, although there is *low confidence* in the models' ability to determine the probability or timing of any such retreat. There is also *medium confidence* (in the light of the limited literature) that Thwaites Glacier is probably less prone to undergo ocean-driven grounding line retreat than its neighbour in the 21st century. No process-based modelling is available on which to be base projections of EAIS glaciers currently losing mass, such as Totten and Cook Glaciers.

Bindschadler et al. (2013) reported a model inter-comparison exercise on the impact of climate change under RCP8.5 on the Antarctic ice

Aanvullend kan ook een filmpje over het opbreken van het Larsen B ijsplateau in een loop opgezet worden op een beeldscherm (zonder geluid). Bv. https://www.youtube.com/watch?v=zIcLuiTt4f4